Robotics and Autonomous Systems 83 (2016) 177–187

Contents lists available at ScienceDirect

Robotics and Autonomous Systems

journal homepage: www.elsevier.com/locate/robot

A high-performance flight control approach for quadrotors using a modified active disturbance rejection technique

Wei Dong [a,b], Guo-Ying Gu [a,*], Xiangyang Zhu [a], Han Ding [a]

[a] State Key Laboratory of Mechanical System and Vibration, School of Mechanical Engineering, Shanghai Jiaotong University, Shanghai, 200240, China
[b] State Key Laboratory of Fluid Power and Mechatronic Systems, Zhejiang University, 310058, China

ARTICLE INFO

Article history:
Received 1 September 2015
Accepted 15 May 2016
Available online 24 May 2016

Keywords:
Quadrotor
Active disturbance rejection control
Input delay
Trajectory tracking
Disturbance observer

ABSTRACT

In practice, the parameters of the flight controller of the quadrotors are commonly tuned experimentally with respect to a certain type of reference, such as the step reference and the unit-ramp reference. In this way, the performance of the flight controller might be affected by the variations of the references in real-time flights. Besides, real-time dynamic effects such as measure noises, external disturbances and input delays, which are usually neglected in the reported works, could easily deteriorate the performances of the flight controllers. This work is thereby motivated to develop a high-performance flight control approach utilizing a modified disturbance rejection technique for the quadrotors suffering from input delays and external disturbances. This control approach is developed in a cascaded structure and the attitude angles are chosen as the pseudo control inputs of the translational flight of the quadrotors. To facilitate the development, the dynamic model of the quadrotors is firstly formulated by including the effects of input delays, and the dynamics of the pseudo control variables are identified through real-time experiments. Based on the identified model, the flight control approach is proposed with a modified active disturbance rejection technique, which consists of a time optimal tracking differentiator, an extended state observer/predictor, and a nonlinear proportional–derivative controller. The tracking differentiator is designed to generate smooth transient profiles for the references, and the extended state observer/predictor is implemented for lumped disturbance estimation and state estimation considering the input delays. With the aid of the tracking differentiator and the extended state observer/predictor, the nonlinear proportional–derivative controller can thereby establish a fast tracking control and effectively reject the estimated disturbances. To verify the feasibilities of this development, comparative tests are carried out in both simulations and experiments. The results show that in the presence of small lumped disturbances, such as the measurement zero-drift, the steady-state errors of the proposed control approach for the ramp responses are less than 2 cm, and in the tests of sinusoidal trajectory tracking, the cross-tracking errors are less than 0.04 m. When with large disturbance airflow that is equivalent to strong breeze, the steady-state error achieved by the proposed flight controller is also less than 10 cm. All of these facts demonstrate the effectiveness of this development.

1. Introduction

In the last decade, numbers of amazing developments of the quadrotors have been presented in the robotics community [1–6]. In view of their excellent performances in the experimental demonstrations, these kinds of unmanned aerial vehicles are hopeful to be adopted for various real-time applications in civil market, such as search, photography and automatic delivery [7,4].

Successful implementation of these applications is closely tied to the performance of the flight controllers [8]. Therefore, numbers of researchers have devoted themselves to develop high performance flight control strategies for the quadrotors in the last few years. Owing to their efforts, a lot of novel controllers such as linear quadratic (LQ) controller [9], backstepping controller, sliding-mode controller [10], and linear matrix inequalities (LMI) based controller [11] have been developed. Unfortunately, most of these controllers are not widely adopted by real-time applications nowadays, and the dominant flight controller of the quadrotors

* Corresponding author.
E-mail addresses: chengquess@sjtu.edu.cn (W. Dong), guguoying@sjtu.edu.cn (G.-Y. Gu), mexyzhu@sjtu.edu.cn (X. Zhu), hding@sjtu.edu.cn (H. Ding).

http://dx.doi.org/10.1016/j.robot.2016.05.005
0921-8890/

is still the classical proportional–integral–derivative (PID) controller [7,12]. These are because the PID controller can be straightforwardly implemented by the practitioners, and the PID controller itself is computationally efficient for the concurrent processing capabilities of the on-board micro control units (MCUs). However, regardless of these superiorities, the PID controller might be not able to well cope with many real-time issues such as communication delays, changing dynamics, and external disturbances [4]. In addition, at least three problems may arise when only conventional PID is adopted for the flight control. Firstly, the integral term of PID controller introduces extra phase lag, which could reduce the stability margin and lead to oscillations when changing disturbances exist. Secondly, as high frequency noises exist in the measurement, the derivative term may not be implementable. Thirdly, as the references of way-point navigations are often constructed with step functions, they are not consistent with the dynamics of the system and the control inputs are required to make sudden jumps for fast tracking of these references [13].

To enhance the performance of the PID controller, several researchers have begun to investigate advanced PID control techniques. Owing to their efforts, some novel controllers, such as fractional order PID (FOPID) controllers [14–16], disturbance observer (DOB) based controllers [17,18] and active disturbance rejection controllers (ADRC) [19,20], have been developed. Among these controllers, the ADRC is the most promising candidate that can well handle the aforementioned drawbacks of the PID controllers. The ADRC consists of three subsystems: a nonlinear PD controller, a tracking differentiator (TD) and an extended state observer (ESO). The TD can smooth the reference by establishing a transient profile, and the ESO can effectively eliminate the measurement noises and estimate the lumped disturbance. With the smoothed reference and the estimated disturbance, the nonlinear PID controller can then establish a fast tracking control. With these functionalities, the ADRC is practically valuable for the flight control of the quadrotors. However, except for some simulation studies [19,20], there is no real-time flight controller developed based on the ADRC in view of the accumulated works. These are because the parameter tuning process as well as the structure of the classic ADRC, especially its nonlinear PD part, are not explicit enough for directly applying in the flight control of the quadrotors, and the performance of the ADRC could also be deteriorated by some real-time dynamic effects. In particular, as reported in [17], input delays caused by the phase lags of the pseudo control inputs [21] and communication delays of the teleoperation [22,23] will introduce extra difficulties for the disturbance rejection of the flight controllers.

To address such challenges, a new control approach, which is based on a modified ADRC (MADRC), is proposed in this paper to enhance the real-time performance of the translational flight control of the quadrotors suffering input delays and external disturbances, and this is conducted as follows. Firstly, the dynamic model of the quadrotors is formulated by including the effects of input delays, and the dynamics of the pseudo control variables are identified through real-time experiments. Subsequently, the flight control approach that contains three subsystems: an ESO/predictor, a TD, and a modified nonlinear PD controller is developed for high performance flight control of the quadrotors. In the ESO/predictor, the dynamics of the pseudo control variables is included for the state estimation, which is thereby possible to eliminate the effects of input delays. With well estimated states, the nonlinear PD controller is then implemented for fast tracking the time optimal reference generated by the TD. Besides, as the nonlinear PD controller is modified into a cascaded structure with less parameters, it is more straightforward for practitioners and less experimental trials are required for parameter tuning. Finally, the superiorities of the proposed control approach over the classic control techniques are demonstrated through comparative tests in both simulations and experiments with a conventional proportional–proportional (P–P) controller and a DOB based proportional–proportional (DOB-P–P) controllers.

The distinctive features of this paper are as follows. Firstly, a high performance flight control approach with the MADRC is proposed, and the parameters tuning rules are also addressed in detail. This control approach can be conveniently implemented in real-time applications, and is robust to the lumped disturbances, input delays and reference variations. Secondly, the improved ESO/predictor provides a computationally efficient approach for state estimation and prediction, and the modified nonlinear PD controller is straightforward for practitioners to apply in real time applications. Finally, real-time experiments are conducted on a quadrotor suffering from measurement zero-drift and external wind gust. In this way, the feasibilities and capabilities of the proposed control approach in real-time applications are extensively studied.

The remaining part of this paper is organized as follows. In Section 2, the quadrotor model is formulated and identified, then Section 3 develops the controller based on the formulated model. Numerical Simulations are thereafter presented in Section 4, and real-time experiments are carried out in Section 5. Section 6 finally concludes this work.

2. Dynamic model

To facilitate the controller design, the dynamic model of the quadrotors is firstly formulated in this section. Based on this model, the pseudo control variables for the translational flight control are then determined, and their dynamics are identified according to real-time experiments.

2.1. Rigid body dynamics

The coordinates and free body diagram of the quadrotors are shown in Fig. 1. According to this diagram, four control inputs can be defined as

$$\begin{aligned} U_1 &= F_1 + F_2 + F_3 + F_4, \qquad U_2 = (F_2 - F_4)L, \\ U_4 &= M_1 - M_2 + M_3 - M_4, \quad U_3 = (F_3 - F_1)L, \end{aligned} \tag{1}$$

where L is the length from the rotor to the center of the mass of the quadrotor, and F_i and M_i are the thrust and torque generated by rotor i ($i \in \{1, 2, 3, 4\}$).

In view of Eq. (1), equations governing dynamics of the quadrotor with respect to the inertial coordinates are generally expressed as [21,24]

$$\begin{cases} \ddot{x} = \dfrac{U_1}{m}(\cos\phi \sin\theta \cos\psi + \sin\phi \sin\psi) \\ \ddot{y} = \dfrac{U_1}{m}(\cos\phi \sin\theta \sin\psi - \sin\phi \cos\psi) \\ \ddot{z} = \dfrac{U_1}{m}\cos\phi \cos\theta - g \\ \ddot{\phi} = \dfrac{U_2}{I_{xx}} + \dot{\theta}\dot{\psi}\left(\dfrac{I_{yy} - I_{zz}}{I_{xx}}\right) - \dfrac{J_R}{I_{xx}}\dot{\theta}\Omega_R \\ \ddot{\theta} = \dfrac{U_3}{I_{yy}} + \dot{\phi}\dot{\psi}\left(\dfrac{I_{zz} - I_{xx}}{I_{yy}}\right) - \dfrac{J_R}{I_{yy}}\dot{\phi}\Omega_R \\ \ddot{\psi} = \dfrac{U_4}{I_{zz}} + \dot{\phi}\dot{\theta}\left(\dfrac{I_{xx} - I_{yy}}{I_{zz}}\right) \end{cases} \tag{2}$$

where x, y, and z are the position of the center of mass in the inertial coordinates; ϕ, θ, and ψ are the attitude; m, I_{xx}, I_{yy}, and I_{zz} are the mass and moments of inertia of the quadrotor, respectively; J_R and Ω_R are the moments of inertia and angular velocity of the propeller blades; and g is the gravity constant.

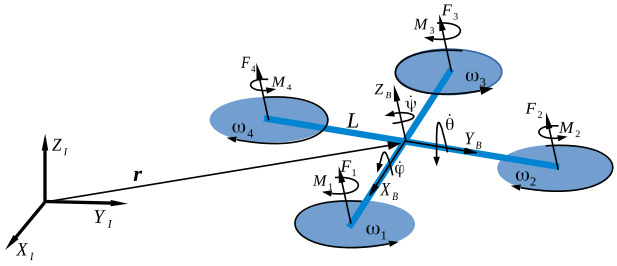

Fig. 1. Free body diagram.

Linearizing Eq. (2) in the near hovering state ($\phi \approx 0,\ \theta \approx 0$), one can obtain

$$\begin{aligned} \ddot{x} &= \frac{U_1}{m}(\theta\cos\psi + \phi\sin\psi), \qquad \ddot{y} = \frac{U_1}{m}(\theta\sin\psi - \phi\cos\psi), \\ \ddot{z} &= \frac{1}{m}U_1 - g, \qquad \ddot{\phi} = \frac{U_2}{I_{xx}}, \qquad \ddot{\theta} = \frac{U_3}{I_{yy}}, \qquad \ddot{\psi} = \frac{U_4}{I_{zz}}. \end{aligned} \tag{3}$$

In this way, U_i ($i \in \{1,\ 2,\ 3,\ 4\}$) can be taken as control inputs to stabilize $z,\ \phi,\ \theta$, and ψ. The stabilized θ and ϕ can be then taken as the pseudo control inputs to stabilize x and y. In view of Eq. (3), one can obtain

$$\begin{bmatrix} \ddot{x} \\ \ddot{y} \end{bmatrix} = \frac{U_1}{m}\boldsymbol{G}\begin{bmatrix} \theta \\ \phi \end{bmatrix} \triangleq \frac{U_1}{m}\boldsymbol{G}\ddot{\boldsymbol{\eta}}, \qquad \boldsymbol{G} = \begin{bmatrix} \cos\psi & \sin\psi \\ \sin\psi & -\cos\psi \end{bmatrix}. \tag{4}$$

Therefore, given desired translational accelerations, one can inversely calculate the required pseudo control inputs as

$$\ddot{\boldsymbol{\eta}}^* \triangleq \begin{bmatrix} \theta^* \\ \phi^* \end{bmatrix} = \left(\frac{U_1}{m}\boldsymbol{G}\right)^{-1}\begin{bmatrix} \ddot{x}^* \\ \ddot{y}^* \end{bmatrix} = \frac{m}{U_1}\boldsymbol{G}\begin{bmatrix} \ddot{x}^* \\ \ddot{y}^* \end{bmatrix} \tag{5}$$

where θ^*, ϕ^*, $\ddot{x}^*$, and $\ddot{y}^*$ are the desired values for θ, ϕ, $\ddot{x}$, and $\ddot{y}$ respectively.

2.2. Dynamics of the pseudo control variables

In this work, the attitude angles, i.e. the pseudo control variables $\boldsymbol{\eta} = [\theta,\ \phi]^T$ utilized in Eq. (5), are stabilized by a proportional–derivative (PD) controller, the details of which can be seen in [17]. Since this controller and the on-board sensors utilized to provide feedback signals have their own dynamics, it is difficult to directly formulate the dynamics of the pseudo control variables based on Eq. (3). In such a case, an experimental identification approach proposed in [25] is adopted to determine the transfer function from $\boldsymbol{\eta}^*$ to $\boldsymbol{\eta}$, and the identified result is

$$P(s) \approx \frac{1}{Ts+1}\mathrm{e}^{-\tau s} \tag{6}$$

with $T = 0.08$ and $\tau = 0.12$.

By taking zero-order hold transform, Eq. (6) can be rewritten as a discrete form as

$$\boldsymbol{\eta}_{(k+1)} \approx a_1\boldsymbol{\eta}_{(k)} + a_2\boldsymbol{\eta}^*_{(k-N_L)} \tag{7}$$

with $a_1 \approx \frac{7}{9}$, $a_2 \approx \frac{2}{9}$, $N_L = 6$ (with step length of 0.02 s) in this work.

Based on Eq. (7), one can obtain

$$\tilde{\boldsymbol{\eta}}_{(k+N)} \approx a_1^N\boldsymbol{\eta}_{(k)} + \sum_{i=1}^{N}(a_1^{i-1}a_2\boldsymbol{\eta}^*_{(k+N-N_L-i)}) \tag{8}$$

where $0 < N \le N_L$.

Utilizing Eq. (8), the response of the attitude at step $k+N$ can be estimated as $\tilde{\boldsymbol{\eta}}_{(k+N)}$ according to the concurrent measurement and the reference sequence $\boldsymbol{\eta}^*$. In this way, when $N = N_L$, the effects of input delays can be theoretically eliminated, and Eq. (8) can be rewritten as

$$\hat{\boldsymbol{\eta}}_{(k)} = \tilde{\boldsymbol{\eta}}_{(k+N_L)} \approx a_1^{N_L}\boldsymbol{\eta}_{(k)} + \sum_{i=1}^{N_L}(a_1^{i-1}a_2\boldsymbol{\eta}^*_{(k-i)}). \tag{9}$$

In the identification experiments, small input delay is also found in U_1, which can be expressed as $U_{1(k+N_U)} = U^*_{1(k)}$, where $U^*_{1(k)}$ is the reference for U_1 and $N_U \approx 2$ in this work.

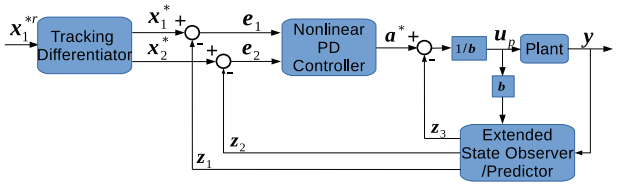

Fig. 2. The topology of the MADRC.

3. Controller design

In this section, the development of the MADRC is presented. As shown in Fig. 2, the MADRC consists of three parts: an ESO/predictor, a TD, and a nonlinear PD controller. To verify the effectiveness of the MADRC, a DOB-P–P controller is also developed for comparison.

3.1. Extended state observer/predictor

The ESO/predictor is developed to provide state estimation as follows. Besides, a conventional Kalman filter is presented to assist the verification of this development.

3.1.1. Extended state observer/predictor

In view of Eq. (2), the model of the quadrotors can be expressed in a compacted form as

$$\begin{cases} \dot{\boldsymbol{x}}_1 = \boldsymbol{x}_2 \\ \dot{\boldsymbol{x}}_2 = \boldsymbol{x}_3 + \boldsymbol{b}\boldsymbol{\eta} \\ \dot{\boldsymbol{x}}_3 = \boldsymbol{g}(t) \end{cases} \tag{10}$$

where $\boldsymbol{b} = U_1/m\boldsymbol{G}$, $\boldsymbol{x}_1 = [x,\ y]^T$, $\boldsymbol{x}_2 = [\dot{x},\ \dot{y}]^T$, and $\boldsymbol{x}_3$ represents the dynamics of the lumped disturbance.

In this way, an ESO can be constructed to estimate the disturbances in the following form [13]

$$\begin{cases} \boldsymbol{e} = \boldsymbol{z}_1 - \boldsymbol{x}_1 \\ \boldsymbol{fe}_1 = \boldsymbol{fal}(\boldsymbol{e}, \alpha_1, \delta), \boldsymbol{fe}_2 = \boldsymbol{fal}(\boldsymbol{e}, \alpha_2, \delta) \\ \dot{\boldsymbol{z}}_1 = \boldsymbol{z}_2 - \beta_1\boldsymbol{e} \\ \dot{\boldsymbol{z}}_2 = \boldsymbol{z}_3 + b\boldsymbol{\eta} - \beta_2\boldsymbol{fe}_1 \\ \dot{\boldsymbol{z}}_3 = -\beta_3\boldsymbol{fe}_2 \end{cases} \tag{11}$$

where α_1 and α_2 are selected as $\alpha_1 = 0.5$ and $\alpha_2 = 0.25$ respectively, and the function $\boldsymbol{fal}(\cdot)$ is designed as

$$\boldsymbol{fal}(e, \alpha, \delta) = \begin{cases} \dfrac{e}{\delta^{1-\alpha}} & |e| \le \delta \\ |e|^{\alpha}sign(e) & |e| > \delta \end{cases} \tag{12}$$

with $sign(\epsilon) \triangleq \epsilon/|\epsilon|$ when $\epsilon \neq 0$, and $sign(0) \triangleq 1$.

Eq. (11) can be rewritten in a discrete form

$$\begin{cases} \boldsymbol{e} = \boldsymbol{z}_{1(k)} - \boldsymbol{x}_{1(k)} \\ \boldsymbol{fe}_1 = \boldsymbol{fal}(\boldsymbol{e}, \alpha_1, \delta), \qquad \boldsymbol{fe}_2 = \boldsymbol{fal}(\boldsymbol{e}, \alpha_2, \delta) \\ \boldsymbol{z}_{1(k+1)} = \boldsymbol{z}_{1(k)} + h\boldsymbol{z}_{2(k)} - \beta_1\boldsymbol{e} \\ \boldsymbol{z}_{2(k+1)} = \boldsymbol{z}_{2(k)} + h(\boldsymbol{z}_{3(k)} + b\boldsymbol{\eta}_{(k)}) - \beta_2\boldsymbol{fe}_1 \\ \boldsymbol{z}_{3(k+1)} = \boldsymbol{z}_{3(k)} - \beta_3\boldsymbol{fe}_2 \end{cases} \tag{13}$$

where h is the step length. According to [13], δ can be selected as $\delta = 2h$, and β_i ($i \in \{1, 2, 3\}$) can be selected as

$$\beta_1 = 1, \qquad \beta_2 = \frac{1}{2h^{0.5}}, \qquad \beta_3 = \frac{2}{25h^{1.2}}. \tag{14}$$

In view of Eq. (8), there exist time delays in the pseudo control inputs. Therefore, the observer constructed by Eq. (13) can be refined with the state prediction as

$$\begin{cases} \boldsymbol{e} = \boldsymbol{z}_{1(k)} - \boldsymbol{x}_{1(k)} \\ \boldsymbol{fe}_1 = \boldsymbol{fal}(\boldsymbol{e}, \alpha_1, \delta), \qquad \boldsymbol{fe}_2 = \boldsymbol{fal}(\boldsymbol{e}, \alpha_2, \delta) \\ \boldsymbol{z}_{1(k+1)} = \boldsymbol{z}_{1(k)} + h\boldsymbol{z}_{2(k)} - \beta_1 \boldsymbol{e} \\ \boldsymbol{z}_{2(k+1)} = \boldsymbol{z}_{2(k)} + h(\boldsymbol{z}_{3(k)} + b\boldsymbol{\eta}_{(k)}) - \beta_2 \boldsymbol{fe}_1 \\ \boldsymbol{z}_{3(k+1)} = \boldsymbol{z}_{3(k)} - \beta_3 \boldsymbol{fe}_2 \\ \tilde{\boldsymbol{z}}_{1(k+n)} = \boldsymbol{z}_{1(k)} + h \sum_{i=1}^{n} \tilde{\boldsymbol{z}}_{2(k+i)} \\ \tilde{\boldsymbol{z}}_{2(k+n)} = \boldsymbol{z}_{2(k)} + h \sum_{i=1}^{n} (\boldsymbol{z}_{3(k)} + b\tilde{\boldsymbol{\eta}}_{(k+i)}) \\ \hat{\boldsymbol{x}}_{1(k)} = \tilde{\boldsymbol{z}}_{1(k+N_L-1)}, \qquad \hat{\boldsymbol{x}}_{2(k)} = \tilde{\boldsymbol{z}}_{2(k+N_L-1)}. \end{cases} \tag{15}$$

In this way, the states $\boldsymbol{x}_{1(k+N_L)}$ and $\boldsymbol{x}_{2(k+N_L)}$ can be estimated by $\hat{\boldsymbol{z}}_{1(k)}$ and $\hat{\boldsymbol{z}}_{2(k)}$ respectively.

In following development, Eq. (13) is referred as ESO, and Eq. (15) is referred as ESO/predictor.

Remark 1. The parameters β_2 and β_3 determine the tracking speed of the observer to the corresponding states. If there values are too small, extra time lag will be introduced into the feedback, but if they are too large, the noises in the measurement of $\boldsymbol{x}_1$ will be amplified in the observation. When tuning these two parameters, one can first adopt the suggested values in Eq. (14), and then adjust them experimentally to obtain the best performance. If real-time flight data can be well collected, the tuning process is suggested to carry out off-line based on the collected data to get rid of potential failures.

3.1.2. Kalman filter

The Kalman Filter is implemented for comparative verification.

Denoting $\boldsymbol{\chi} = [x, y, \dot{x}, \dot{y}]^T$, the dynamics of the quadrotor can be rewritten in a discrete form with step $\tau_{(k)}$, and a measurement can be created as

$$\begin{aligned} \boldsymbol{\chi}_{(k+1)} &= \boldsymbol{A}_{(k)}\boldsymbol{\chi}_{(k)} + \boldsymbol{B}_{(k)}\boldsymbol{u}_{(k)} + \boldsymbol{w}_{(k)} \\ \boldsymbol{\zeta}_{(k)} &= \boldsymbol{H}_{(k)}\boldsymbol{\chi}_{(k)} + \boldsymbol{v}_{(k)} \end{aligned} \tag{16}$$

where $\boldsymbol{A}_{(k)} = \begin{bmatrix} \boldsymbol{I}_{2\times2} & \tau_{(k)}\boldsymbol{I}_{2\times2} \\ \boldsymbol{0}_{2\times2} & \boldsymbol{I}_{2\times2} \end{bmatrix}$, $\boldsymbol{B}_{(k)} = \begin{bmatrix} \frac{1}{2}\tau_{(k)}^2\boldsymbol{I}_{2\times2} \\ \tau_{(k)}\boldsymbol{I}_{2\times2} \end{bmatrix}$, $\boldsymbol{H}_{(k)} = \boldsymbol{I}_{4\times4}$, $\boldsymbol{u}_{(k)} = [\frac{U_{1(k-U_T)}\hat{\theta}_{(k)}}{m}, -\frac{U_{1(k-U_T)}\hat{\phi}_{(k)}}{m}]^T$, and $\boldsymbol{w}_{(k)}$ and $\boldsymbol{v}_{(k)}$ are the noises with $p(\boldsymbol{w}) \sim N(\boldsymbol{0}, \boldsymbol{Q})$ and $p(\boldsymbol{v}) \sim N(\boldsymbol{0}, \boldsymbol{R})$ respectively.

Then the Kalman filter is designed with standard procedure as [26]

$$\hat{\boldsymbol{\chi}}_{(k)}^- = \boldsymbol{A}_{(k)}\hat{\chi}_{(k)} + \boldsymbol{B}_{(k)}\boldsymbol{u}_{(k-1)} \tag{17}$$

$$\boldsymbol{P}_{(k)}^- = \boldsymbol{A}_{(k)}\boldsymbol{P}_{k-1}\boldsymbol{A}_{(k)}^T + \boldsymbol{Q} \tag{18}$$

$$\boldsymbol{K}_{(k)} = \boldsymbol{P}_{(k)}^-\boldsymbol{H}_{(k)}^T(\boldsymbol{H}_{(k)}\boldsymbol{P}_{(k)}^-\boldsymbol{H}^T + \boldsymbol{R})^{-1} \tag{19}$$

$$\hat{\boldsymbol{\chi}}_{(k)} = \hat{\boldsymbol{\chi}}_{(k)}^- + \boldsymbol{K}_k(\boldsymbol{\zeta}_{(k)} - \boldsymbol{H}_{(k)}\hat{\boldsymbol{\chi}}_{(k)}^-) \tag{20}$$

$$\boldsymbol{P}_{(k)} = (\boldsymbol{I} - \boldsymbol{K}_{(k)}\boldsymbol{H}_{(k)})\boldsymbol{P}_{(k)}^-. \tag{21}$$

3.2. Tracking differentiator

In view of Eq. (10), the position control can be expressed as a double integral process

$$\begin{cases} \dot{\boldsymbol{x}}_1 = \boldsymbol{x}_2 \\ \dot{\boldsymbol{x}}_2 = \boldsymbol{f}(\boldsymbol{u}) \triangleq \boldsymbol{v}. \end{cases} \tag{22}$$

In order to establish a fast tracking control for Eq. (22), a time-optimal control problem for this process can be stated as

$$\begin{aligned} \min \quad & J = \min \int_0^T dt \\ s.t. \quad & \dot{\boldsymbol{x}}_1 = \boldsymbol{x}_2, \dot{\boldsymbol{x}}_2 = \boldsymbol{v} \\ & \boldsymbol{x}_1(0) = \boldsymbol{x}_{10}, \boldsymbol{x}_2(0) = \boldsymbol{x}_{20} \\ & \boldsymbol{x}_1(T) = \boldsymbol{x}_1^{*r}, \boldsymbol{x}_2(T) = 0 \\ & |\boldsymbol{v}| \le v_{max}. \end{aligned} \tag{23}$$

The analytic solution for Eq. (23) can be determined as [27]

$$\begin{cases} \dot{\boldsymbol{x}}_1 = \dot{\boldsymbol{x}}_2 \\ \dot{\boldsymbol{x}}_2 = -v_{max}sign\left(\boldsymbol{x}_1 - \boldsymbol{x}_1^{*r} + \frac{\boldsymbol{x}_2|\boldsymbol{x}_2|}{2v_{max}}\right). \end{cases} \tag{24}$$

Based on the profile determined by Eq. (24), the discrete form of the desired state trajectory for $\boldsymbol{x}_1$ and $\boldsymbol{x}_2$ can be constructed as [13]

$$\begin{cases} \boldsymbol{x}_{1(k+1)}^* = \boldsymbol{x}_{1(k)}^* + h\boldsymbol{x}_{2(k)}^* \\ \boldsymbol{x}_{2(k+1)}^* = \boldsymbol{x}_{2(k)}^* + h\boldsymbol{fst}(\boldsymbol{x}_{1(k)}^* - \boldsymbol{x}_1^{*r}, r_0, h) \end{cases} \tag{25}$$

where h is the step length, $\boldsymbol{x}_1^{*r}$ is the reference, r_0 determines the tracking speed, and $\boldsymbol{fst}(\cdot)$ is defined as

$$\begin{aligned} \boldsymbol{fst}(e_1, x_2^*, r_0, h) &= \begin{cases} -r_0 sign(a), & |a| > d \\ -r_0\frac{a}{d}, & |a| \le d \end{cases} \\ a &= \begin{cases} x_2^* + \frac{a_0 - d}{8}sign(y), & |y| > d_0 \\ x_2^* + \frac{y}{h}, & |y| \le d_0 \end{cases} \end{aligned} \tag{26}$$

with $d = r_0h$, $d_0 = hd$, $y = \boldsymbol{e}_1 + hx_2^*$, $a_0 = \sqrt{d^2 + 8r_0|y|}$.

When $\boldsymbol{x}_1^{*r}$ changes with time, one can replace $\boldsymbol{x}_1^{*r}$ with $\boldsymbol{x}_{1(k)}^{*r}$ in Eq. (25). By utilizing Eq. (25) and (26), one can expect $\boldsymbol{x}_1^* \to \boldsymbol{x}_1^{*r}$, $\boldsymbol{x}_2^* \to \dot{\boldsymbol{x}}_1^{*r}$, and high frequency noises in $\boldsymbol{x}_1^{*r}$ can be effectively filtered out [13].

Remark 2. As Eq. (25) is developed based on the optimal control problem Eq. (23), one should thoroughly consider the boundary of the input $\boldsymbol{v}$, which is actually the acceleration of the quadrotors. In order to obtain good performance, the tracking speed r_0 should not exceed the reachable acceleration of the quadrotors.

3.3. Nonlinear PD controller

For the ADRC, the nonlinear PD controller is commonly proposed as [13]

$$\boldsymbol{u}_n = k_p\boldsymbol{fal}(\boldsymbol{e}_1, \alpha_p, \delta) + k_d\boldsymbol{fal}(\boldsymbol{e}_2, \alpha_d, \delta) \tag{27}$$

with $0 \le \alpha_p \le 1$ and $\alpha_d \ge 1$, and $\boldsymbol{e}_1$ and $\boldsymbol{e}_2$ are the position tracking error and velocity tracking error respectively.

In Eq. (27), when the tracking errors of the position and velocity are both large ($\boldsymbol{e}_i > 1$), the second term $k_d\boldsymbol{fal}(\boldsymbol{e}_2, \alpha_d, \delta)$ dominates the control, while when the tracking errors of the position and velocity are both small ($\boldsymbol{e}_i \ll 1$), the first term $k_p\boldsymbol{fal}(\boldsymbol{e}_1, \alpha_p, \delta)$ dominates the control. In this way, the control strategy firstly stabilizes the slow dynamic variables, i.e. the position, and when the position tracking errors are small enough, the tracking errors of the fast dynamic variables (velocity) can be rapidly compressed.

However, there are at least two facts that hinder directly utilizing this nonlinear controller in this work. Firstly, at least five parameters should be tuned to obtain good performance. As the dynamic model of the quadrotors might be inaccurate, this may take plenty of experiments. Secondly, Eq. (27) actually constructs the control input based on the combined tracking errors of the position and velocity, which may make the original problem behave similarly to an under-actuated problem [28]. In this work,

this nonlinear controller of Eq. (27) is slightly modified to obtain more explicit forms as follows.

Firstly, the position error signal and the velocity signal are defined as

$$\bar{\boldsymbol{e}}_1 = \boldsymbol{x}_1^* - \hat{\boldsymbol{z}}_1, \qquad \bar{\boldsymbol{e}}_2 = \boldsymbol{v}^* - \hat{\boldsymbol{z}}_2 \tag{28}$$

where $\boldsymbol{v}^*$ is a virtual control input to stabilize $\boldsymbol{x}_1$.

Then a negative feedback can be constructed as

$$\boldsymbol{v}^* = \boldsymbol{x}_2^* + k_p \boldsymbol{fal}(\bar{\boldsymbol{e}}_1, \alpha_p, \delta), \quad \boldsymbol{a}^* = k_v \bar{\boldsymbol{e}}_2 \tag{29}$$

where $\boldsymbol{a}^*$ is the desired value for the acceleration.

Then substituting the observed disturbances, the pseudo control input of this nonlinear PD controller is constructed as

$$\boldsymbol{u}_p = (\boldsymbol{a}^* - \boldsymbol{z}_3)/\boldsymbol{b} \tag{30}$$

where $\boldsymbol{u}_p = [\theta^*, \phi^*]^T$.

As Eqs. (13), (25) and (27) is developed according to the classic ADRC, the controller constructed with Eqs. (15), (25) and (29) will be referred as MADRC in the following discussions.

Remark 3. From the construction of the tracking differentiator, it can be seen that if the generated $\boldsymbol{x}_2^*$ is well tracked, the desired path $\boldsymbol{x}_1^*$ will be also well stabilized. Therefore, $\boldsymbol{v}^*$ in Eq. (29) is constructed with two terms: the desired $\boldsymbol{x}_2^*$, and a negative feedback compensation $c_1 \boldsymbol{fal}(\bar{\boldsymbol{e}}_1, \alpha_p, \delta)$. With this design, the original nonlinear PD controller is converted to a cascaded structure with three parameters to tune, which will make the controller be easier to implement, yet the inner velocity control loop is the same as a conventional proportional controller. Although we emphasis these merits of the modified nonlinear PD controller, it should be noted that the controller represented in Eq. (29) is still inherently the form of Eq. (27) with $\alpha_d = 1$.

3.4. DOB-P–P controller

To compare the performance of the developed controller, a DOB-P–P controller is developed in a similar manner to [17] as follows

$$\begin{aligned} \boldsymbol{v}^* &= k_{cp}(\boldsymbol{x}_{1d} - \boldsymbol{x}_1) \\ \boldsymbol{u}_{cp} &= (k_{cd}(\boldsymbol{v}^* - \boldsymbol{x}_2) - \hat{\boldsymbol{w}})/\boldsymbol{b} \end{aligned} \tag{31}$$

where $\hat{\boldsymbol{w}} = (\boldsymbol{x}_2 - \int_0^t \boldsymbol{b}\boldsymbol{u}_{cp}\mathrm{d}t)/t$ is the estimated lumped disturbance.

It can be seen that when $\hat{\boldsymbol{w}}$ is set to be zero, Eq. (31) is reduced to a P–P controller, which will be also adopted for comparison in the following simulations and experiments.

4. Simulations

To preliminarily verify the effectiveness of the developed controllers, numeric simulations are conducted in this section. All of the simulations run in the Matlab/Simulink environment at a frequency of 50 Hz, and the parameters adopted in the simulations are shown in Table 1. These parameters are tuned based on the integral time absolute error criteria (ITAEC) [29] when the controllers follow the unit ramp reference. To investigate the effects of the noises in the real-time flight, white noises with amplitude of 0.02 are introduced to the dynamics of the attitude, and white noises with amplitude of 0.005 m are introduced in the measurement of the position. It should be noted that although the amplitude of noises in the position measurement seems small, but when with 50 Hz control frequency, these noises will be amplified up to 0.25 m/s in the velocity estimation of the quadrotor. On the other hand, the following simulations and experiments will demonstrate the effects of these noises are quite significant compared to the steady-state error of this control strategy. Therefore, the measurement noises introduced in this section have realistic meanings considering the high accuracy of the position tracking control strategy development by this work.

Table 1
The parameters adopted for simulations.

k_p	6.00	k_d	0.00	k_v	6.00
α_p	0.75	α_d	1.00	δ	0.10
β_1	1.00	β_2	3.54	β_3	8.75
r_0	2.50	h	0.02	d	0.04
k_{cp}	2.50	k_{cd}	4.00	M_w	0.50

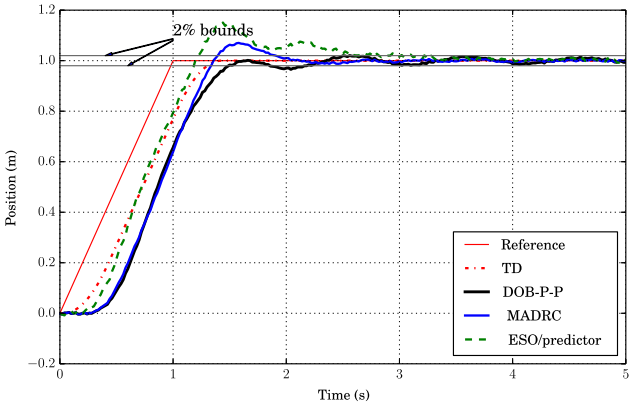

Fig. 3. The comparative results for the MADRC controller.

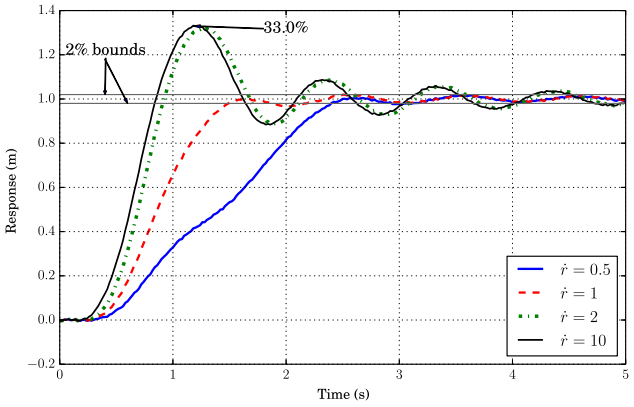

Fig. 4. The responses of the DOB-P–P controller to different ramp references.

As aforementioned, since the development of this work is mainly aimed to improve the performance of the horizontal position (x and y directions) control, the following tests are also carried only in these two directions. Considering the fact that the dynamics in x and y directions are symmetric, only the plot in x direction, without repeatedly labeled in the figures, is illustrated for each test.

As shown in Fig. 3, the responses of the MADRC and the DOB-P–P controller to the unit ramp reference are illustrated. Since the parameters are tuned with respect to the same ramp reference, the performances of these two controllers are nearly the same. The intermediate reference generated by the tracking differentiator presents an 'S'-shape, ensuring smooth flights of the quadrotor. As there are input delays and the reference is a gradually changed ramp reference, significant delays, approximately 0.3 s, are observed in the responses of both MADRC and DOB-P–P, and this will be also illustrated in the following discussions.

With the tuned parameters, these two controllers are then conducted to follow four non-unit ramp references. As shown in Figs. 4 and 5, when the slope of the reference increases, large

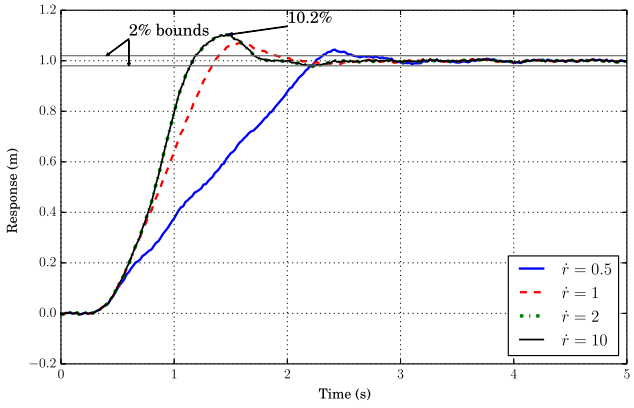

Fig. 5. The responses of the MADRC to different ramp references.

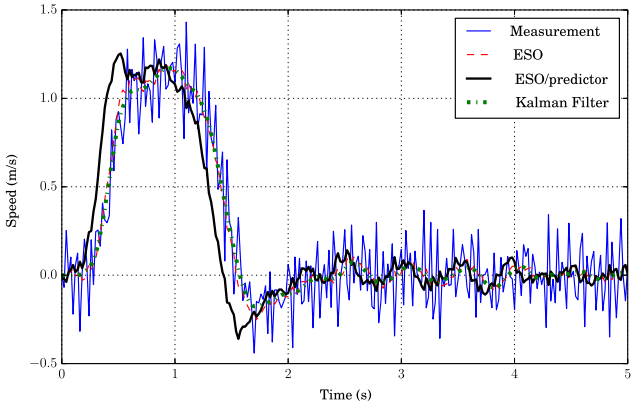

Fig. 6. The velocity observed by the ESO when following the unit ramp reference.

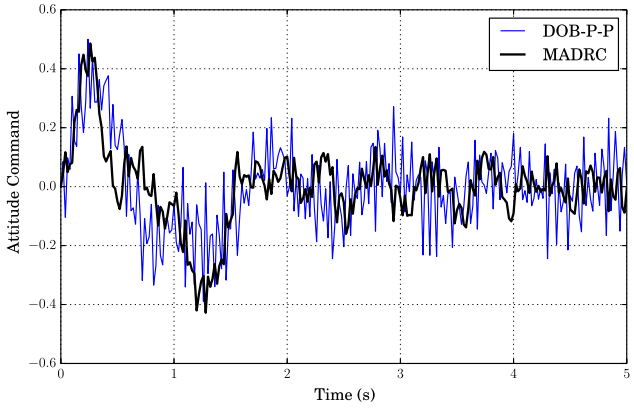

Fig. 7. The history of attitude command with respect to the unit slope ramp reference.

overshoots are found in the responses of the DOB-P–P controller, and the resulted oscillations make the controller unable to stabilize the position with the given time of simulation. In contrast, the overshoot of the MADRC is much smaller than that of the DOB-P–P controller. Besides, in all of these tests, the settling time of the MADRC is less than 2.5 s and steady-state error is less than 2%. All of these results imply that the MADRC can provide steady performance regardless of the variation of the references, which demonstrates its superiority over the conventional DOB-based controller.

The feasibilities of the ESO/predictor in the MADRC can be firstly observed in Fig. 3. It can be seen that the estimated position

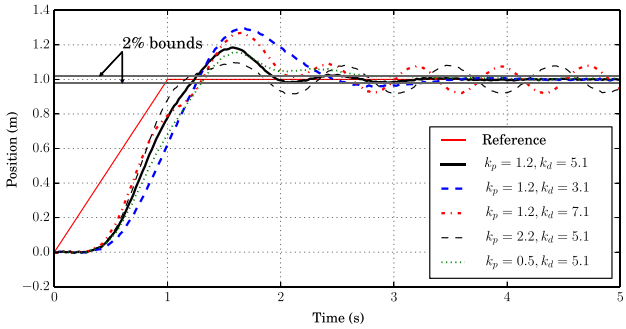

Fig. 8. The unit ramp response of the classic ADRC.

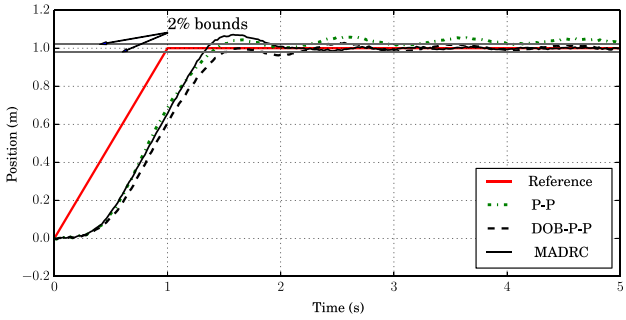

Fig. 9. The response of the comparative simulations when subject to external disturbances.

is ahead of the actual response with nearly a steady amount of time, which means the ESO/predictor could effectively eliminate the effects of the input delays. A further comparison of the performances of the ESO, ESO-predictor and the Kalman Filter is illustrated in Fig. 6, where the estimated velocities corresponding to Fig. 3 are plotted. It can be seen that the ESO only shows similar capabilities with Kalman filter in tracking the original signal and filter out the noises, but with ESO/predictor, the estimation can further eliminate the effects of input delay. Besides, as the noises in the signals are filtered out, the derivative term in the PID control is thereby implementable and the pseudo control input generated by the MADRC controller is much smoother than its counterpart, which is illustrated in Fig. 7. Owing to this improvement, the chattering in the attitude control can be effectively alleviated as well.

To demonstrate the advantages of the MADRC compared to classic ADRC, the unit ramp response of the ADRC is illustrated in Fig. 8. It should be noted that at least five parameters should be tuned for the ADRC, this commonly requires plenty of experimental trials. In this work, these parameters are set as the same with MADRC except k_p and k_d. Then, utilizing ITAEC, k_p and k_d are tuned as $k_p = 1.2$ and $k_d = 5.1$. In Fig. 8, the responses of the controller with different parameters are also plotted. It can be seen that compared to the MADRC, the overshoots and oscillations of the ADRC are much more perceptible.

To verify the capabilities of disturbance rejection, an external disturbance with amplitude of 0.5 m/s^2 is introduced in the simulation. The responses of the developed MADRC and its counterparts are illustrated in Fig. 9. It can be seen that pure P–P controller cannot stabilize the position within the 2% error boundary, whereas both DOB-P–P controller and MADRC controller can effectively reject the disturbances and stabilize the position with a steady-state error of 2%.

All of the results from the simulations demonstrate that the developed MADRC can well track varying references, and effectively reject external disturbances, measurement noises and input delays.

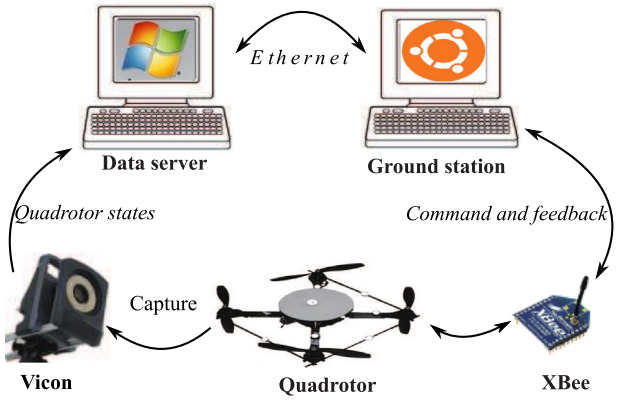

Fig. 10. The quadrotor test bed.

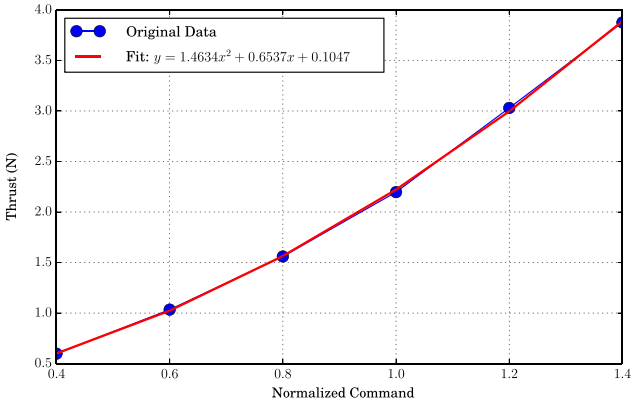

Fig. 11. The relation between the thrust and the command.

5. Experiments

5.1. Experimental setup

The experiments are conducted in an indoor test bed, as shown in Fig. 10, where a commercial quadrotor platform, namely the Hummingbird quadrotor, is adopted. Since quadrotor has served in the test bed over six months, perceptible deformations are observed on the motor booms. In such a case, the thrust generated by each motor, and thus the overall thrust U_1, is not always coincident with the body-fixed $\mathbf{Z}_B$ direction. However, the on-board inertial measurement unit still measure the attitude and acceleration of the quadrotor in the body-fixed frame $\mathcal{B}(X_B - Y_B - Z_B)$, as shown in Fig. 1. In this way, the effects of external disturbances are well introduced in the way of modeling mismatches and measurement zero-drifts (approximate 2.5° zero-drift in the attitude). The quadrotor communicates with a ground control station via a couple of XBee wireless routers at a frequency of 50 Hz. To improve the real-time performance of the flight control, the control station runs on a Linux (Ubuntu 14.04) operating system and is constructed in the Simulink environment. This control station fetches the position data of the quadrotor from the data server of the VICON motion capture system, and the velocity of the quadrotor is then obtained by taking derivative of the position data. The motion capture system runs at a frequency of 200 Hz, and the motion of quadrotor is captured by kinematic fitting of the reflective markers attached on the quadrotor. The development of this test bed can be seen in [30].

5.2. Parameters

In view of Eq. (5), m and U_1 are identified firstly in this section. m is measured to be 0.69 kg by a digital scale, and as shown in Fig. 11, the relation between the command and the thrust of an individual rotor is well fit by a quadratic equation, where the command is normalized into (0, 2). The detailed identification of the rotor can be seen in [17]. In this way, given the desired thrust $T_r = U_1/4$, the required command is calculated as

$$T_c = \frac{-0.6537 + \sqrt{5.8536T_r - 0.1855}}{2.9268}. \tag{32}$$

The parameters for the controllers are preliminarily selected according to the simulation results, then refined by the trial and error method when following the unit ramp reference. The selected parameters in the experiments are shown in Table 2.

Table 2
The parameters adopted for experiments.

k_p	2.00	k_d	0.00	k_v	5.00
α_p	0.90	α_d	1.00	δ	0.04
β_1	1.00	β_2	5.00	β_3	0.80
r_0	2.50	h	0.02	d	0.04
k_{cp}	2.00	k_{cd}	3.50	M_w	0.50

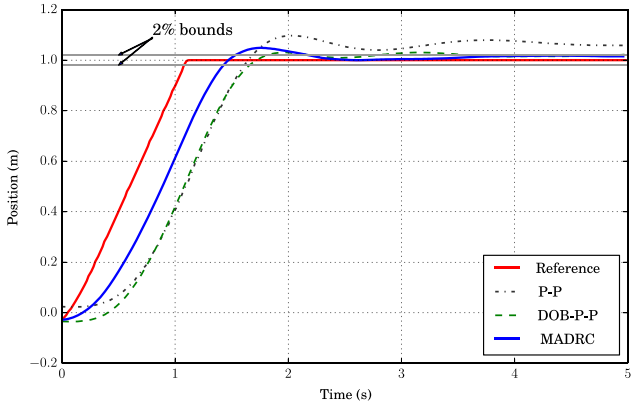

Fig. 12. The comparative experimental results for the MADRC controller.

5.3. Experimental results

The MADRC, DOB-P–P controller and P–P controller are firstly implemented to follow a unit ramp reference. As shown in Fig. 12, barely with P–P controller, the steady state error is approximately 8%. In contrast, both the MADRC and the DOB-P–P controller can well eliminate the effects of external disturbance and the steady-state error is less than 2%. However, different from the results in the simulations, the response of the DOB-P–P controller is slightly slower than that of the MADRC. This might be because that compared to the simulations, the control gains are selected relatively conservative in the experiments, and the response speed of the DOB-P–P controller is more sensitive to these decreased control gains than the nonlinear PD based MADRC. It should be noted that in the real-time experiments, as it is commonly difficulty to precisely manipulate the quadrotor to an identified initial point, there are perceptible initial tracking errors at the start point in Fig. 12. As these errors are less than 0.05 m in this work, it is believed that the verification feasibilities of the developed control strategy will not affected by these deviations, considering the following additional experimental tests.

The velocities estimated by the ESO/predictor and Kalman filter are shown in Fig. 13. It can be seen that both the ESO/predictor and the Kalman filter can well track the original signal and filter out noises, and the ESO/predictor also shows its capability in state prediction. In this way, similar to simulations, the pseudo control input generated by the MADRC is smoother than its counterpart, which is illustrated in Fig. 14. In Fig. 14, the quadrotor needs to

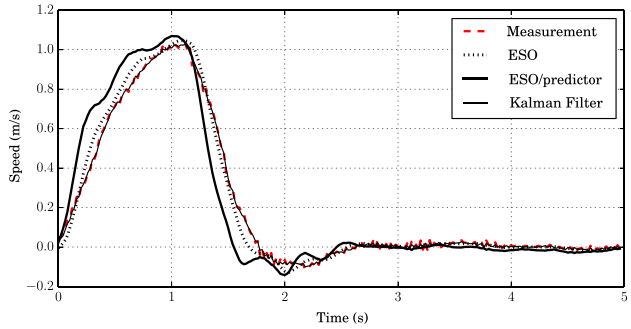

Fig. 13. The observed velocity.

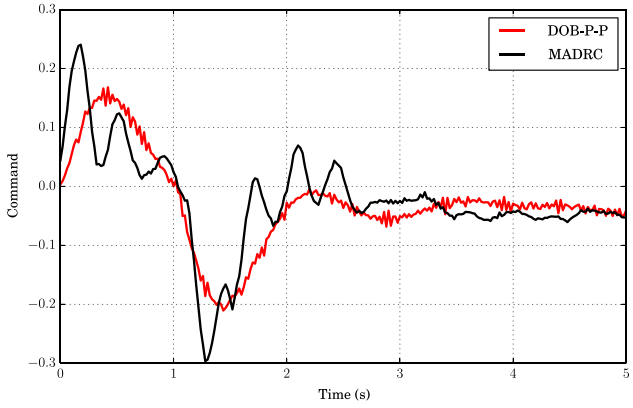

Fig. 14. The attitude command.

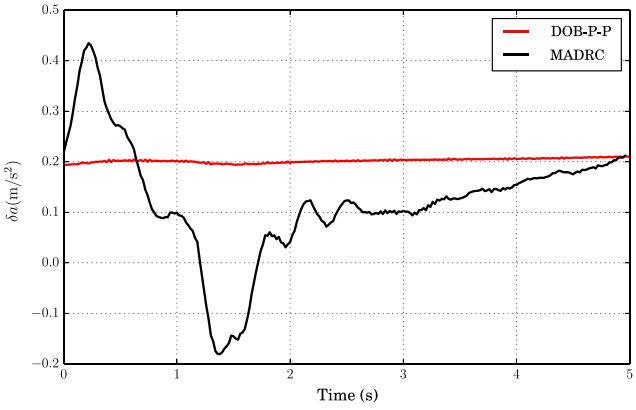

Fig. 15. The observed disturbance.

establish a non-zero attitude to achieve the steady-state, which confirms an approximate 0.04 (2.5°) measurement zero-drift on the adopted quadrotor.

The disturbances observed by the MADRC and the DOB-P–P controller are shown in Fig. 15. It can be seen that the observed value of the DOB-P–P controller behaves in an integral manner, as expected from the development of Eq. (31). In contrast, the MADRC is more sensitive to the dynamic changing, which is caused by nonlinear dynamics and un-modeled factors. In the estimation of the disturbance, it should also be noted that since the measurement noises could be introduced by several sources in real-time flights, β_3 is selected much smaller than that adopted in the simulations to get avoid of amplifying these noises.

Figs. 16 and 17 show the responses of the MADRC and the DOB-based P–P controller to different types of ramp references. It can be seen that the DOB-P–P controller shows large oscillations and steady-state errors when the slope of the ramp reference increases, while the MADRC can always provide steady performances. This

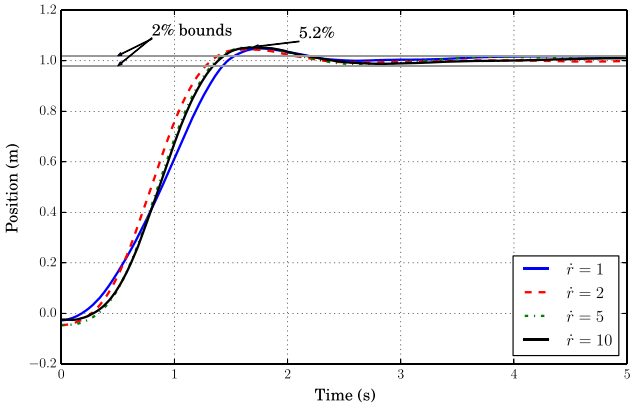

Fig. 16. The response of MADRC under ramp references with different slope.

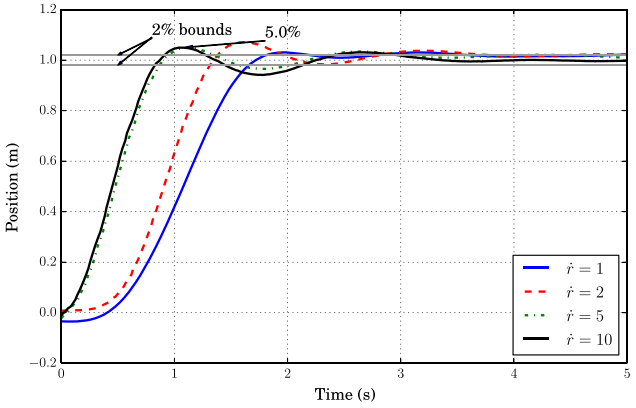

Fig. 17. The responses of DOB-P–P controller under ramp references with different slope.

is because the tracking differentiator in the MADRC is capable of autonomously smoothing the original reference trajectory into an 'S'-shaped transient trajectory, as demonstrated in Fig. 3. In this way, even when the slope of the original ramp reference changes greatly, the MADRC can always utilize the nonlinear PD controller to track the dynamically consistent 'S'-shaped curve with the aid of the ESO/predictor, thus establishes a relatively steady performance. In contrast, in view of the development of the DOB-P–P controller, its response speed is much more closely related to the slope of the original reference trajectory which is dynamically inconsistent, thus leads to oscillation, overshooting and thereby presents much different behaviors.

To compare the performance of the developed MADRC to its classic counterpart, numbers of additional experiments are conducted to verify the performance of the ADRC. As aforementioned, it is very difficult to find the global optimal control gains for the ADRC, since there are five parameters required to tune simultaneously. In this work, with the trial and error method, the α_p, α_d and δ are selected the same as that adopted by the MADRC, and several different values are selected for parameters k_p and k_v. In this way, the responses of the ADRC following a unit ramp reference are illustrated in Fig. 18. Similar to the results shown in the simulation, the responses of the classic ADRC show large overshoots and steady-state errors. In addition, it also takes longer time for the ADRC to reach its steady-state. This is mainly because there is no explicit velocity control loop, and the state estimation accuracy in the ADRC is also comparatively lower than that in the MADRC. Those facts imply that the MADRC effectively improves the performance of the quadrotor in real-time flights.

By artificially introducing external wind gust, an additional comparative experiment is conducted to verify the disturbance

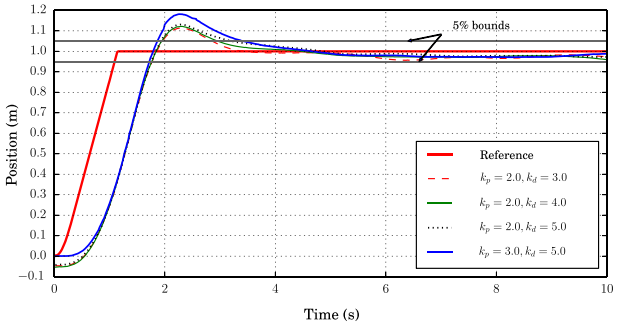

Fig. 18. The responses of the classic ADRC with different control gains.

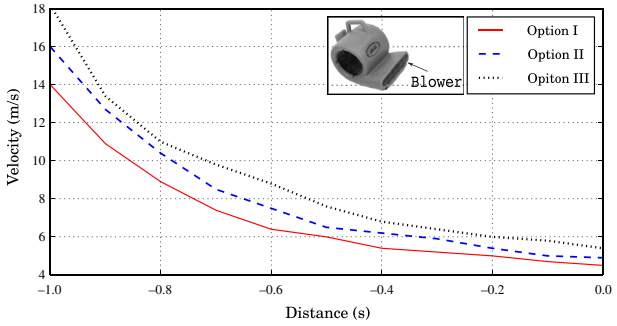

Fig. 19. The velocity distribution in the centerline of the air flow produced by the draft blower.

rejection capability of the MADRC as follows. First, an industrial draft blower (Jie Ba BF533) is set up at $(-1.4, 0, 0.5)$ facing in the positive X direction in the test bed. There are totally three velocity options on the adopted draft blower. For each option, the velocity of produced wind is measured by this work with a ventilation meter (TSI VelociCalc 9535) at the centerline of the airflow at every 0.1 m along the X-axis. The measured distribution is illustrated in Fig. 19. It should be mentioned that there are fluctuations in the airflow, and the maximum fluctuations observed in the measurement are about 5%.

With those introduced external disturbances, the quadrotor is controlled to follow a unit ramp reference in the negative X-axis direction along the centerline of the airflow disturbance. The responses of three flight controllers under three different airflow disturbances are illustrated in Fig. 20. As there exist disturbance airflows at the origin (with velocity approximately 5 m/s), the quadrotor does not start at $X = 0$ in each test (although the initial set-point is $X = 0$). Examining this start point, it can be seen that the MADRC controller achieves smaller deviations to the set-point compared to its counterpart, which means it already shows better robustness to external disturbances at the very beginning stage of this flight control process.

It should be noted that although the DOB-based controller shows good performance in [17] when the velocity of the external wind gust is relatively small, it shows slight different behavior when the disturbance airflow is much larger. The airflow velocities at $X = -0.8$ are approximately 8.9 m/s (Option I), 10.4 m/s (Option II), and 11.0 m/s (Option III). Such airflows are equivalent to the fresh breeze and strong breeze in the real world, which are quite large considering the thrust of the quadrotor itself. In such a case, the MADRC can still guarantee 10% steady-state error in the disturbance option I and option II, while its counterpart cannot achieve the same performance. Although the performance of the MADRC deteriorates in disturbance option III, it is still significantly better than the DOB-P–P controller and the P–P controller. All of those results indicate the MADRC can

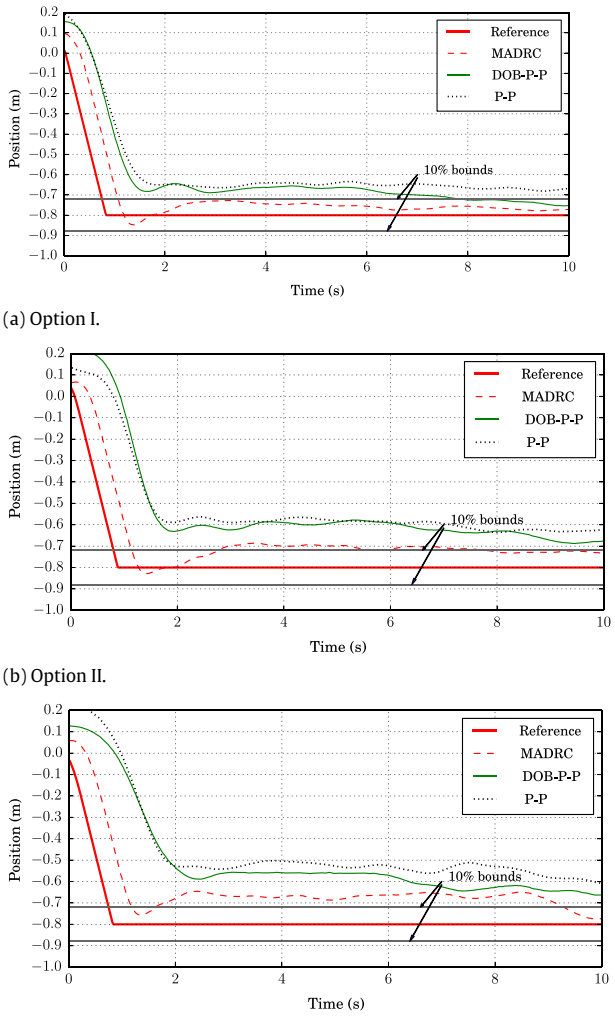

Fig. 20. The responses of the MADRC, DOB-P–P and P–P controllers with different disturbance airflow options.

achieve better performance than the aforementioned conventional controllers, especially when large external disturbances exist.

To further verify the performance of the MADRC regarding different references, the quadrotor is conducted to follow sinusoidal references given by $y = \sin(\Omega t)$. As shown in Fig. 21, the responses and errors of the MADRC and DOB-P–P controller are plotted for a single period of the sinusoidal references. It can be seen that the along-tracking errors of the developed MADRC are smaller than its counterpart both when $\dot{\Omega} = 1$ and when $\dot{\Omega} = 0.5$, as shown in Fig. 21(b). This is because in the tracking process, the time lag of the MADRC is smaller than that of the DOB-P–P controller, as verified by aforementioned experiments. Besides, as illustrated in Fig. 21(c), the cross-tracking errors of the MADRC are less than 0.04 m, whereas those of the DOB-P–P controller are greater than 0.05 m, which also shows the superiority of the MADRC. It should be noted that as this work aim to track 'unknown' reference trajectory, the dynamic tracking error in this way is larger than some other existing tracking methods with respect to known trajectory. This is because when the desired trajectory is known, one could generate the desired input as a feedforward, and in such a case, the quadrotor can more closely track the desired trajectory with high accuracy.

All of these results demonstrate that the MADRC can well eliminate the effects of input delays, reject disturbances and

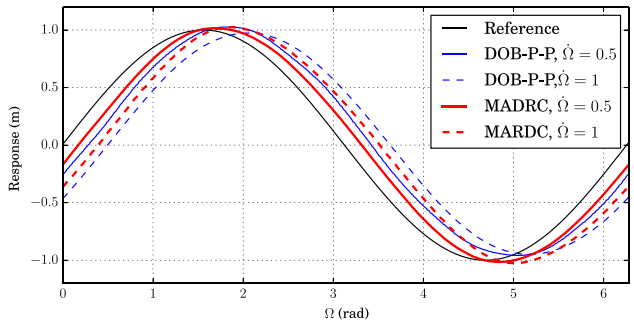

(a) Responses.

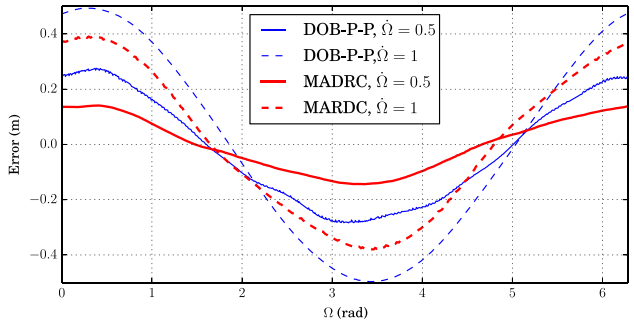

(b) Along-tracking errors.

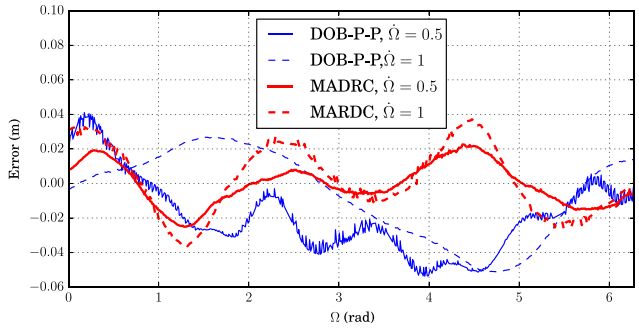

(c) Cross-tracking errors.

Fig. 21. The responses to sinusoidal references and the corresponding error plots.

track changing references, thus show better performances than conventional PID controllers and DOB-based controllers.

6. Conclusion

In this work, a high performance flight control approach using a modified disturbance rejection technique has been proposed for the quadrotors. To facilitate the development of this approach, the dynamics of the quadrotors considering external disturbances and input delays are firstly formulated and identified through real-time experiments. Utilizing the identified dynamic model, the control approach containing three subsystems: a TD, an ESO/predictor, and a nonlinear PD controller is proposed for flight control of the quadrotors. The TD can generate intermediate references with smooth transient profiles, thus get avoid of large overshoots and oscillations. The ESO/predictor can effectively filter out the measurement noises, eliminate the effects of input delays, and estimate the lumped disturbance. The estimated disturbance can then be utilized by the nonlinear PD controller for disturbance rejection. In this way, a fast tracking control that is robust to external disturbances, input delays and reference variations can be established. In addition, as this control approach is developed in a similar manner to the conventional PID controller, it is easy and straightforward for practitioners to apply in real-time applications.

Comparative simulations and experiments with conventional control strategies have verified these features, and experimental results show that the proposed control approach significantly enhances the performance of flight control when applied to a quadrotor with measurement zero-drift and external wind gust. With measurement zero-drift (approximate 2.5° in the attitude), the position of the quadrotor is well stabilized with steady-state error of 2 cm within 2.5 s, and in the tests of sinusoidal trajectory tracking, the cross-tracking errors are less than 0.04 m. When with disturbance airflow (speed ranges from approximately 9 m/s to 11 m/s), the quadrotor can be also stabilized with steady-state error of 10 cm. All of these facts demonstrate the feasibilities and advantages of this development.

Acknowledgments

This work was funded by Open Foundation of the State Key Laboratory of Fluid Power Transmission and Control (No. GZKF-201510).

References

[1] M. Hehn, R. D'Andrea, A flying inverted pendulum, in: Proceedings of IEEE International Conference on Robotics and Automation, 2011, pp. 763–770.
[2] Q. Lindsey, D. Mellinger, V. Kumar, Construction with quadrotor teams, Auton. Robots 33 (3) (2012) 323–336.
[3] D. Mellinger, V. Kumar, Minimum snap trajectory generation and control for quadrotors, in: Proceedings of IEEE International Conference on Robotics and Automation, 2011, pp. 2520–2525.
[4] V. Kumar, N. Michael, Opportunities and challenges with autonomous micro aerial vehicles, Int. J. Robot. Res. 31 (11) (2012) 1279–1291.
[5] M. Muller, S. Lupashin, R. D'Andrea, Quadrocopter ball juggling, in: Proceedings of IEEE International Conference on Intelligent Robots and Systems, 2011, pp. 5113–5120.
[6] W. Dong, G.-Y. Gu, X. Zhu, H. Ding, Solving the boundary value problem of an under-actuated quadrotor with subspace stabilization approach, J. Intell. Robot. Syst. (2014) 1–13.
[7] H. Lim, J. Park, D. Lee, H. Kim, Build your own quadrotor: Open-source projects on unmanned aerial vehicles, IEEE Robot. Autom. Mag. 19 (3) (2012) 33–45.
[8] M. Abdolhosseini, Y.M. Zhang, C.A. Rabbath, An efficient model predictive control scheme for an unmanned quadrotor helicopter, J. Intell. Robot. Syst. (2012) 1–12.
[9] S. Bouabdallah, A. Noth, R. Siegwart, Pid vs lq control techniques applied to an indoor micro quadrotor, in: Proceedings of the IEEE/RSJ International Conference on Intelligent Robots and Systems, Vol. 3, 2004, pp. 2451–2456.
[10] S. Bouabdallah, Design and control of quadrotors with application to autonomous flying (Ph.D. thesis), 2007.
[11] T. Ryan, H. Kim, Lmi-based gain synthesis for simple robust quadrotor control, IEEE Trans. Autom. Sci. Eng. 10 (4) (2013) 1173–1178.
[12] N. Michael, D. Mellinger, Q. Lindsey, V. Kumar, The grasp multiple micro-uav testbed, IEEE Robot. Autom. Mag. 17 (3) (2010) 56–65.
[13] J. Han, From pid to active disturbance rejection control, IEEE Trans. Ind. Electron. 56 (3) (2009) 900–906.
[14] I. Podlubny, Fractional-order systems and pi/sup/spl lambda//d/sup/spl mu//-controllers, IEEE Trans. Automat. Control 44 (1) (1999) 208–214.
[15] M.Ö Efe, Neural network assisted computationally simple pi d control of a quadrotor uav, IEEE Trans. Ind. Inform. 7 (2) (2011) 354–361.
[16] Y. Luo, L. Di, J. Han, H. Chao, Y. Chen, Vtol uav altitude flight control using fractional order controllers, in: Proceedings of the 4th IFAC Workshop on Fractional Differentiation and Its Application, 2010, pp. 1–6.
[17] W. Dong, G.-Y. Gu, X. Zhu, H. Ding, High-performance trajectory tracking control of a quadrotor with disturbance observer, Sensors Actuators A 211 (2014) 67–77. http://dx.doi.org/10.1016/j.sna.2014.03.011.
[18] S. Jung, An impedance force control approach to a quad-rotor system based on an acceleration-based disturbance observer, J. Intell. Robot. Syst. 73 (1–4) (2014) 175–185. http://dx.doi.org/10.1007/s10846-013-9929-0. URL http://dx.doi.org/10.1007/s10846-013-9929-0.
[19] C. Peng, Y. Tian, Y. Bai, X. Gong, C. Zhao, Q. Gao, D. Xu, Adrc trajectory tracking control based on pso algorithm for a quad-rotor, in: Proceedings of the IEEE Conference on Industrial Electronics and Applications, 2013, pp. 800–805.
[20] X. Gong, Y. Tian, Y. Bai, C. Zhao, Trajectory tacking control of a quad-rotor based on active disturbance rejection control, in: Proceedings of the IEEE International Conference on Automation and Logistics, 2012, pp. 254–259.
[21] Z.T. Dydek, A.M. Annaswamy, E. Lavretsky, Adaptive control of quadrotor uavs: A design trade study with flight evaluations.
[22] Z. Li, X. Cao, Y. Tang, R. Li, W. Ye, Bilateral teleoperation of holonomic constrained robotic systems with time-varying delays, IEEE Trans. Instrum. Meas. 62 (4) (2013) 752–765.
[23] Z. Li, Y. Xia, F. Sun, Adaptive fuzzy control of multilateral cooperative teleoperation for multiple robotic manipulators under random time delays, IEEE Trans. Fuzzy Syst. 22 (2) (2014) 437–450.

[24] S. Bouabdallah, P. Murrieri, R. Siegwart, Design and control of an indoor micro quadrotor, in: Proceedings of the IEEE International Conference on Robotics and Automation, Vol. 5, 2004, pp. 4393–4398.
[25] W. Dong, G. Gu, X. Zhu, H. Ding, Modeling and control of a quadrotor uav with aerodynamic concepts, in: Proceedins of the International Conference on Intelligent Unmanned Systems, 2013, pp. 377–382.
[26] S.G. Mohinder, P.A. Angus, Kalman Filtering: Theory and Practice Using Matlab, John Wiley & Sons, Inc., New York, 2001, pp. 178–181.
[27] D.P. Bertsekas, D.P. Bertsekas, D.P. Bertsekas, D.P. Bertsekas, Dynamic Programming and Optimal Control, Vol. 1, Athena Scientific Belmont, Massachusetts, 1995.
[28] L. Márton, A.S. Hodel, B. Lantos, J.Y. Hung, Underactuated robot control: comparing lqr, subspace stabilization, and combined error metric approaches, IEEE Trans. Ind. Electron. 55 (10) (2008) 3724–3730.
[29] Y. Chen, et al., System Simulation Techniques with MATLAB and Simulink, John Wiley & Sons, 2013.
[30] W. Dong, G.-Y. Gu, X. Zhu, H. Ding, Development of a quadrotor test bed—modelling, parameter identification, controller design and trajectory generation, Int. J. Adv. Robot. Syst. 12 (2015) 7.

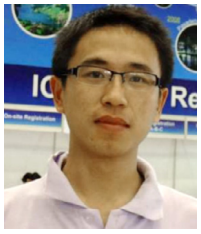

Wei Dong received the B.E. degree and the Ph.D. degree in mechanical engineering from Shanghai Jiao Tong University, Shanghai, China, in 2009 and 2015, respectively. Dr. Dong is currently working as a postdoctoral research fellow with School of Mechanical Engineering at Shanghai Jiao Tong University. His research interest is on the modeling and control of unmanned aerial vehicles.

Guo-Ying Gu received the B.E. degree (with honors) in Electronic Science and Technology, and the Ph.D. degree (with honors) in Mechatronic Engineering from Shanghai Jiao Tong University, Shanghai, China, in 2006 and 2012, respectively.

Dr. Gu was a Visiting Scholar at Concordia University, Montreal, QC, Canada, and National University of Singapore, Singapore. Supported by the Alexander von Humboldt Foundation, he was a Humboldt Fellow at University of Oldenburg, Oldenburg, Germany. Since October 2012, he has been working at Shanghai Jiao Tong University, where he is currently appointed as an Associate Professor with School of Mechanical Engineering. His research interests include soft/continuum robots, smart material actuated devices and unmanned aerial vehicles. He is the author or co-author of over 40 publications, which have appeared in journals, as book chapters and in conference proceedings.

Dr. Gu is a member of the American Society of Mechanical Engineers. Now Dr. Gu serves as Associate Editor of International Journal of Advanced Robotic Systems. He has also served for several international conferences as Associate Editor or a program committee member.

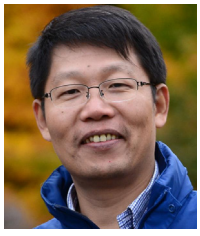

Xiangyang Zhu received the B.S. degree from the Department of Automatic Control Engineering, Nanjing Institute of Technology, Nanjing, China, in 1985, the M.Phil. degree in instrumentation engineering and the Ph.D. degree in automatic control engineering, both from Southeast University, Nanjing, China, in 1989 and 1992, respectively. From 1993 to 1994, he was a postdoctoral research fellow with Huazhong University of Science and Technology, Wuhan, China. He joined the Department of Mechanical Engineering as an associate professor, Southeast University, in 1995. Since June 2002, he has been with the School of Mechanical Engineering, Shanghai Jiao Tong University, Shanghai, China, where he is currently a Changjiang Chair Professor and the director of the Robotics Institute. His current research interests include robotic manipulation planning, human–machine interfacing, and biomechatronics. Dr. Zhu received the National Science Fund for Distinguished Young Scholars in 2005.

Han Ding received his Ph.D. degree from Huazhong University of Science and Technology (HUST), Wuhan, China, in 1989. Supported by the Alexander von Humboldt Foundation, he was with the University of Stuttgart, Germany from 1993 to 1994. He worked at the School of Electrical and Electronic Engineering, Nanyang Technological University, Singapore from 1994 to 1996. He has been a Professor at HUST ever since 1997 and is now Director of State Key Lab of Digital Manufacturing Equipment and Technology there.

Dr. Ding was a "Cheung Kong" Chair Professor of Shanghai Jiao Tong University from 2001 to now. Dr. Ding acted as an Associate Editor of IEEE Trans. on Automation Science and Engineering(TASE) from 2004 to 2007. He was elected as member of Chinese Academy of Sciences in 2013. Currently, he is a editor of TASE and a Senior Editor of IEEE Robotics and Automation Letters. His research interests include robotics, multi-axis machining and control engineering.